THE EUROPEAN PHYSICAL JOURNAL PLUS

(Italian Society of Physics)

Impact factor: 3.911

Accepted August 18th 2021

NUMERICAL SIMULATION OF THERMAL MANAGEMENT DURING NATURAL CONVECTION IN A POROUS TRIANGULAR CAVITY CONTAINING AIR AND HOT OBSTACLES

Veena Chandanam[1], C. Venkata Lakshmi[1], K. Venkatadri[2*], **O. Anwar Bég**[3] and V. Ramachandra Prasad[4]

[1]*Department of Applied Mathematics, Sri Padmavathi Mahila Visvavidyalayam, Tirupati 517502,* ***India.***

[2]*Department of Mathematics, Sreenivasa Institute of Technology and Management Studies, Chittoor-517127,* ***India.***

[3]*Multi-Physical Engineering Sciences Group, Aeronautical/Mechanical Engineering, Salford University, School of Science, Engineering and Environment (SEE), Manchester, M54WT,* ***UK***

[4]*Department of Mathematics, School of Advanced Sciences, Vellore Institute of Technology, Vellore – 6322014,* ***India****.*

Corresponding Author: venkatadri.venki@gmail.com

ABSTRACT

A numerical study is presented of laminar viscous magnetohydrodynamic natural convection flow in a triangular shaped porous enclosure filled with electrically conducting air and containing two hot obstacles. The mathematical model is formulated in terms of dimensional partial differential equations. The pressure gradient term is eliminated by using the vorticity-stream ($\omega-\psi$) function approach. The emerging dimensionless governing equations are employed by the regular finite difference scheme along with thermofluidic boundary conditions. The efficiency of the obtained computed results for isotherms and streamlines are validated via comparison with previously published work. The impact of physical parameters on streamlines and temperature contours for an extensive range of Rayleigh number (Ra=10^3-10^5), Hartmann magnetohydrodynamic number (Ha=5-30), Darcy parameter (Da=0.0001-0.1) for fixed Prandtl number (Pr = 0.71) are considered. Numerical results are also presented for local and average Nusselt numbers along the hot base wall. Interesting features of the thermofluid behaviour are revealed. At lower Rayleigh number the isotherms are generally parallel to the inclined wall and only distorted substantially near the obstacles at the left vertical adiabatic wall; however, with increasing *Rayleigh number*, this distortion is magnified in the core zone and simultaneously warmer zones expand towards the inclined cold wall. The simulations are relevant to magnetic materials processing and hybrid magnetic fuel cells.

KEYWORDS: *Magnetic materials processing; triangular enclosure; permeable medium; natural convection; finite difference solution; internal obstacles.*

NOMENCLATURE

Dimensional

x	*co-ordinate parallel to base of enclosure (m)*
y	*co-ordinate perpendicular to base of enclosure (m)*
g	*acceleration due to gravity (m/s^2)*
L	*length of base and vertical walls of triangular enclosure (m)*
u	*x-direction velocity (m/s)*
y	*y-direction velocity (m/s)*
B_o	*magnitude of applied magnetic field (Tesla)*
K	*permeability of the porous medium (m^2)*
p	*hydrodynamic pressure (Pa)*
K	*effective thermal conductivity of fluid saturated porous medium (W/mK)*
t	*time (s)*
T	*temperature (K)*
C_p	*isobaric specific heat (J/kgK)*
σ	*electrical conductivity of fluid (Siemens/m)*
β	*thermal expansion coefficient of fluid (/K)*
μ	*dynamic viscosity of fluid (kg/ms)*
ν	*kinematic viscosity of fluid (m^2/s)*
ρ	*fluid density at reference temperature (kg/m^3)*
α	*thermal diffusivity of fluid-saturated porous medium ((m^2/s)*
q	*heat flux (W/m^2)*

Dimensionless

τ	*dimensionless time*
Ha	*Hartmann hydromagnetic number*
Da	*Darcy number*
Pr	*Prandtl number*
Nu	*Nusselt number*
Ra	*Rayleigh number*
X	*dimensionless x co-ordinate*
Y	*dimensionless y co-ordinate*
U	*dimensionless u velocity*

V *dimensionless v velocity*

θ *dimensionless temperature*

ψ *stream function*

ω *vorticity function*

Subscripts and Superscripts

$( )_h$ *Hot wall (base)*

$( )_c$ *Cold wall (inclined)*

1. INTRODUCTION

Buoyancy driven flow within enclosures filled with pure fluids, permeable media and/or different geometrical configurations has been scrutinized by a number of investigators. Most works are concerned with examination of heat transfer in cavities (square, rectangular, trapezium etc). Processing in magnetic fields is a rapidly expanding research area with a wide range of promising applications in materials science, development and design. Numerous research centers dedicated to materials research and processing in magnetic fields have been created around the world. However triangular enclosures also have significant applications in solar energy collectors, various thermal ducts, convection in reservoir sidearms, building and thermal insulation systems, air gaps, crystal growth technologies etc. As such many investigations have been reported for triangular enclosure convection for different working fluids e.g. air, helium, water, nanofluids and liquid metals (gallium) with multiple physical effects including magnetohydrodynamics, entropy generation, porous media, mass transfer, radiative heat transfer etc. Liu *et al.* [1] entropy based simulation convection within a tilted triangular cavity under the effect of horizontal magnetic field. Their result indicated 12% enhancement in heat transfer and 13% enhancement in entropy generation with a sizeable increment in Rayleigh number. They further noted that when magnetic field strength (as simulated by Hartmann number) is increased by 6.5%, an 8% decrement in heat transfer and entropy generation is observed and furthermore for a high inclination angle there is a significant reduction in Nusselt number. Das *et al.* [2] studied entropy generation in convective flow in thermally efficient regular and inverted isosceles triangular designs and also a square cavity utilizing double heaters located at different positions on each side wall. They showed that when the heaters are positioned at the centre and lower half of the triangle, a massive rate of heat

distribution and lower rate of entropy generation is observed. Mahain *et al.* [3] used both theoretical correlations and experimental approaches to estimate Nusselt number values and heat distribution coefficient ratios in free convection of Silica-water nanofluid inside both square and triangular enclosure. In their observation the average Nusselt number shows a similar trend with maximum difference of only 4.5% in the absence of measured thermophysical properties. Feroz *et al.* [4] described a numerical study of mixed convective hydromagnetic flow and heat distribution within a lid-driven triangular cavity containing a circular obstacle, showing that there is considerable augmentation of heat propagation with increasing Richardson number whereas the converse response is computed with increment in Hartmann (magnetic) number. Mohsen Izadi [5] numerically simulated the transient free convection in a hybrid nanofluid filled in a triangular cavity containing permeable media for different nanoparticle shapes and volume fractions. He noted that a rise in volume fraction of nanoparticles inhibits heat propagation in hybrid nanofluids, whereas in the case of unitary nanofluid the convection heat transfer is improved with greater nanoparticles volume fraction. Selimefendigil *et al.* [6] explored the heat mechanism in Cu-water liquid within a triangular enclosure containing a rotating insulated circular cylinder, observing that both flow rate and heat transfer rate are successfully controlled with judicious selection of the rotational speed of the circular cylinder. Kent *et al.* [7] analysed the natural convection in a triangular enclosure with various thermal boundary conditions. Further studies on buoyancy/mixed convection fluid flow inside various enclosure geometries (rectangular cavity, square cavity, triangular cavity) are described in the references [8–14] wherein many different computational techniques have been used including finite element methods, ANSYS FLUENT finite volume methods etc.

In recent years thermal engineers have increasingly explored various heating approaches within enclosures containing porous media since porous materials offer significant advantages in terms of heat transfer control, insulation, flow regulation etc. Das *et al.* [15] explored natural convection in porous enclosures (square and triangle) with discreate heating, computing thermal mixing characteristics within the closed domain with the help of Bejan heatline concept. Ahmed *et al.* [16] carried out a numerical examination of natural convective laminar flow in a triangular enclosure containing a heat source. Li *et al.* [17] simulated the hydromagnetic power-law rheological buoyancy driven flow in an inclined triangular enclosure with discreate heating portion on the boundaries. They showed that with increment in Rayleigh number (thermal buoyancy parameter), heat transfer rate for pseudoplastic (shear-thinning fluid) is significantly boosted as is the associated entropy generation rate. Yesiloz and Aydin

[18] adopted the finite volume method (ANSYS FLUENT) to examine the laminar natural convection water in a triangular domain, presenting extensive results for flowpatterns and temperature lines for dissimilar values of buoyancy number and obtaining good correlation with experiments. Ahmed *et al*. [19] studied finite difference based technique to simulate the effect of a heat source (located on the base wall) on natural convection in copper-water nanofluids within a triangular enclosure with a cold inclined wall, filled with a Darcian porous medium. They used the Tiwari-Das nanoscale model and showed that average Nusselt number is enhanced initially with increasing nanoparticle (copper) volume fraction but inhibited at higher volume fractions. They also showed that there is a substantial modification induced in the average Nusselt number with location and extent of the heat source along the bottom wall. Chowdhury *et al.* [20] used a Galerkin weighted residual finite element method to examine the natural convection mechanism of heat and mass distribution in an alumina-water nanofluid triangular enclosure containing porous media with heat source effects. They noted that average Nusselt number and Sherwood number are elevated with increasing Rayleigh number, heat generation parameter, Lewis number and solid volume fraction. Al-Farhany *et al.* [37] investigate double-diffusive natural convection in a complex enclosure containing two equilateral triangular obstacles. Ali Doostali and Marzieh Rezazadeh [38] used the lattice Boltzmann method to investigate the natural convection heat transfer in a cavity with three heaters are situated at the bottom wall. In this study, a square cavity with air inside is considered.

Motivated by developments in magnetic materials processing [21-25], the present article investigates magnetohydrodynamic natural convection of air in a saturated porous triangular enclosure featuring two isothermal hot bodies placed along the right-angled wall. Such a configuration has to the authors' knowledge not yet received the attention in the scientific literature. Heated internal obstacles have been shown to offer significant advantages in thermofluid regulation techniques in materials processing and also fuel cells [26-27]. Several investigators are discussed flow and heat transfer with mono obstacle and not considered triangular enclosure. So, the objective is to provide a deeper insight into the momentum and heat transfer characteristics in such an enclosure under a transverse magnetic field, thereby furnishing useful benchmark data for possible laboratory studies and other computational simulations. A numerical solution is developed based on the vorticity formulation and a finite difference scheme is developed. Comprehensive visualization of streamline and isotherm contours and also Nusselt numbers, is included for the effects of magnetic field, Darcy

parameter and thermal Rayleigh number. Validation with the special case of non-magnetic convection in the absence of a porous medium as studied by Basak *et al.* [28] is included confirming the accuracy of the present computational approach.

2. MATHEMATICAL FORMULATION

The schematic diagram **Fig. 1(a)** illustrates the regime of interest i.e. a two-dimensional triangular enclosure containing two hot obstacles. Unsteady laminar viscous incompressible natural convection of electrically conducting air filled porous right-angle triangular enclosure is considered. The lengths of the height and width of the enclosure is L. The hypotenuse i.e., inclined cold wall is maintained at a low temperature T_c, the base wall is sustained at high temperature T_h. and the vertical wall is an adiabatic boundary. An external magnetic field is imposed parallel to the x-axis direction and gravitational acceleration acts perpendicular to the x-axis. All the thermophysical properties are considered as constant except density. Magnetic induction and Ohmic dissipation effects are ignored. The porous medium has constant permeability in all directions (isotropic). The density is approximated by the help of Boussinesq approximation and heat generation/absorption, viscous dissipation, and radiation effects are neglected. By virtue of the above assumptions, the governing conservation partial nonlinear differential equations (i.e., continuity, *X, Y- momentum and energy*) in Cartesian form may be presented as [29-35]:

a)

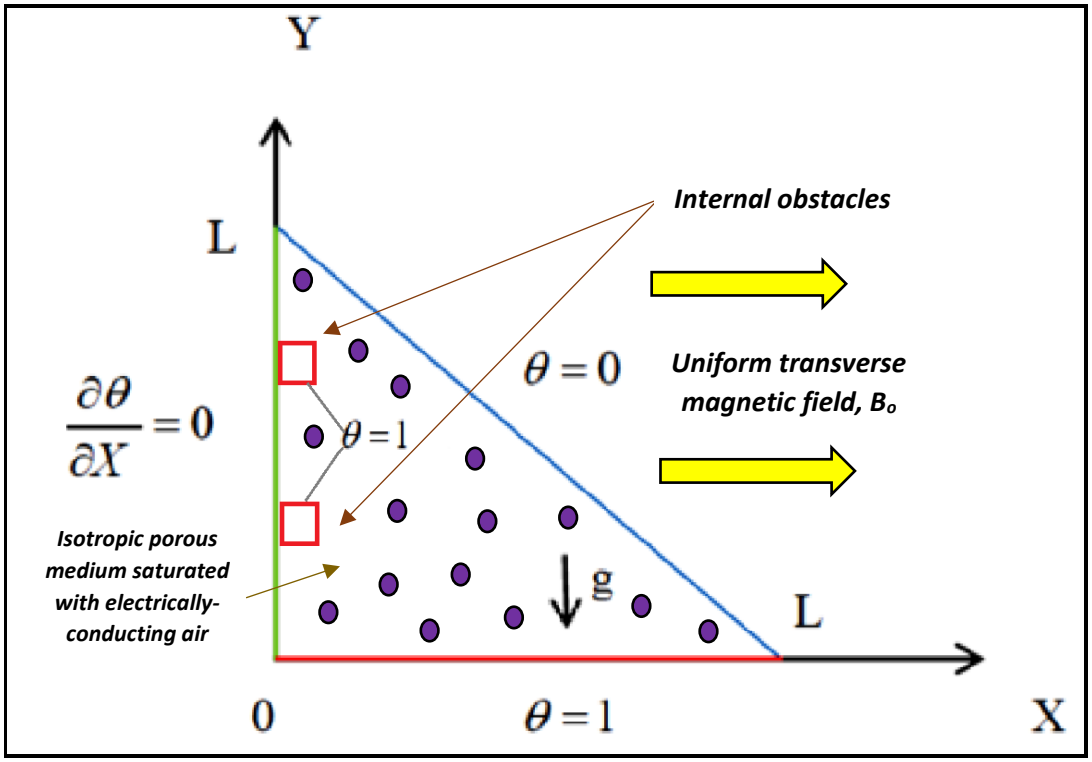

b)

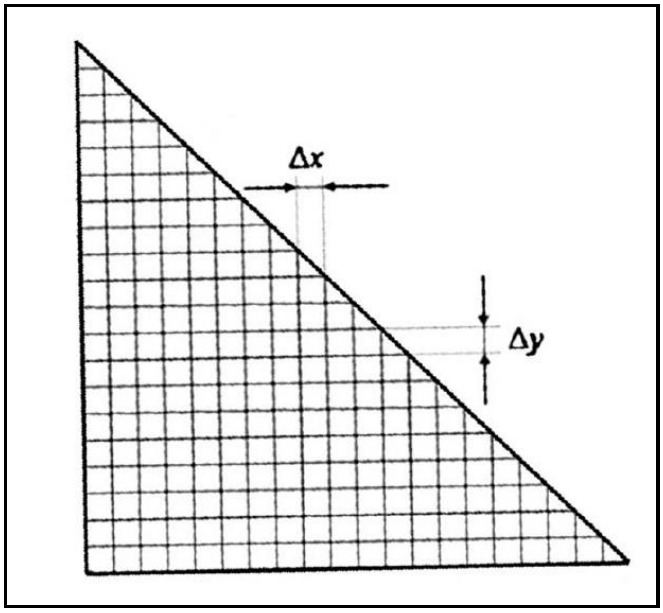

Fig. 1 (a) Schematic diagram (b) mesh

$$\frac{\partial u}{\partial x} + \frac{\partial v}{\partial y} = 0 \tag{1}$$

$$\frac{\partial u}{\partial t} + u\frac{\partial u}{\partial x} + v\frac{\partial u}{\partial y} = -\frac{1}{\rho}\frac{\partial p}{\partial x} + \upsilon\left(\frac{\partial^2 u}{\partial x^2} + \frac{\partial^2 u}{\partial y^2}\right) - \frac{\upsilon}{K}u \tag{2}$$

$$\frac{\partial v}{\partial t}+u\frac{\partial v}{\partial x}+v\frac{\partial v}{\partial y}=-\frac{1}{\rho}\frac{\partial p}{\partial y}+\upsilon\left(\frac{\partial^2 v}{\partial x^2}+\frac{\partial^2 v}{\partial y^2}\right)-\frac{\upsilon}{K}v-\frac{\sigma}{\rho}B_0^2 v+g\beta_T\left(T-T_c\right) \tag{3}$$

$$\frac{\partial T}{\partial t}+u\frac{\partial T}{\partial x}+v\frac{\partial T}{\partial y}=\alpha\left(\frac{\partial^2 T}{\partial x^2}+\frac{\partial^2 T}{\partial y^2}\right) \tag{4}$$

It is noteworthy that the Darcian drag components arise in both the primary (x-direction) and secondary (*y*-direction) momentum conservation Eqns. (2) and (3) whereas the Lorentzian magnetohydrodynamic body force only features in the secondary momentum Eqn. (3).

The following dimensionless variables are introduced:

$$\tau=\frac{t\alpha}{L^2},X=\frac{x}{L},Y=\frac{y}{L},U=\frac{uL}{\alpha},V=\frac{vL}{\alpha}$$

$$\theta=\frac{T-T_c}{T_h-T_c},\ P=\frac{pL^2}{\rho\alpha^2}, \tag{5}$$

The boundary conditions at the three walls of the enclosure are defined as follows:

On the vertical wall	on bottom wall	on the inclined wall
x=0, u = v = 0, $\frac{\partial T}{\partial x}=0$	y=0, u=v=0, $T=T_h$	u=v=0, $T=T_c$

(6)

Using Eqn. (5) in Eqns. (1) – (4), the transformed dimensionless governing equations are:

$$\frac{\partial U}{\partial X}+\frac{\partial V}{\partial Y}=0 \tag{7}$$

$$\frac{\partial U}{\partial \tau}+U\frac{\partial U}{\partial X}+V\frac{\partial U}{\partial Y}=-\frac{\partial P}{\partial X}+\Pr\left(\frac{\partial^2 U}{\partial X^2}+\frac{\partial^2 U}{\partial Y^2}\right)-\frac{\Pr}{Da}U \tag{8}$$

$$\frac{\partial V}{\partial \tau}+U\frac{\partial V}{\partial X}+V\frac{\partial V}{\partial Y}=-\frac{\partial P}{\partial Y}+\Pr\left(\frac{\partial^2 V}{\partial X^2}+\frac{\partial^2 V}{\partial Y^2}\right)-\frac{\Pr}{Da}V-HA^2\Pr V+Ra.\Pr\theta \tag{9}$$

$$\frac{\partial \theta}{\partial \tau}+U\frac{\partial \theta}{\partial X}+V\frac{\partial \theta}{\partial Y}=\left(\frac{\partial^2 \theta}{\partial X^2}+\frac{\partial^2 \theta}{\partial Y^2}\right) \tag{10}$$

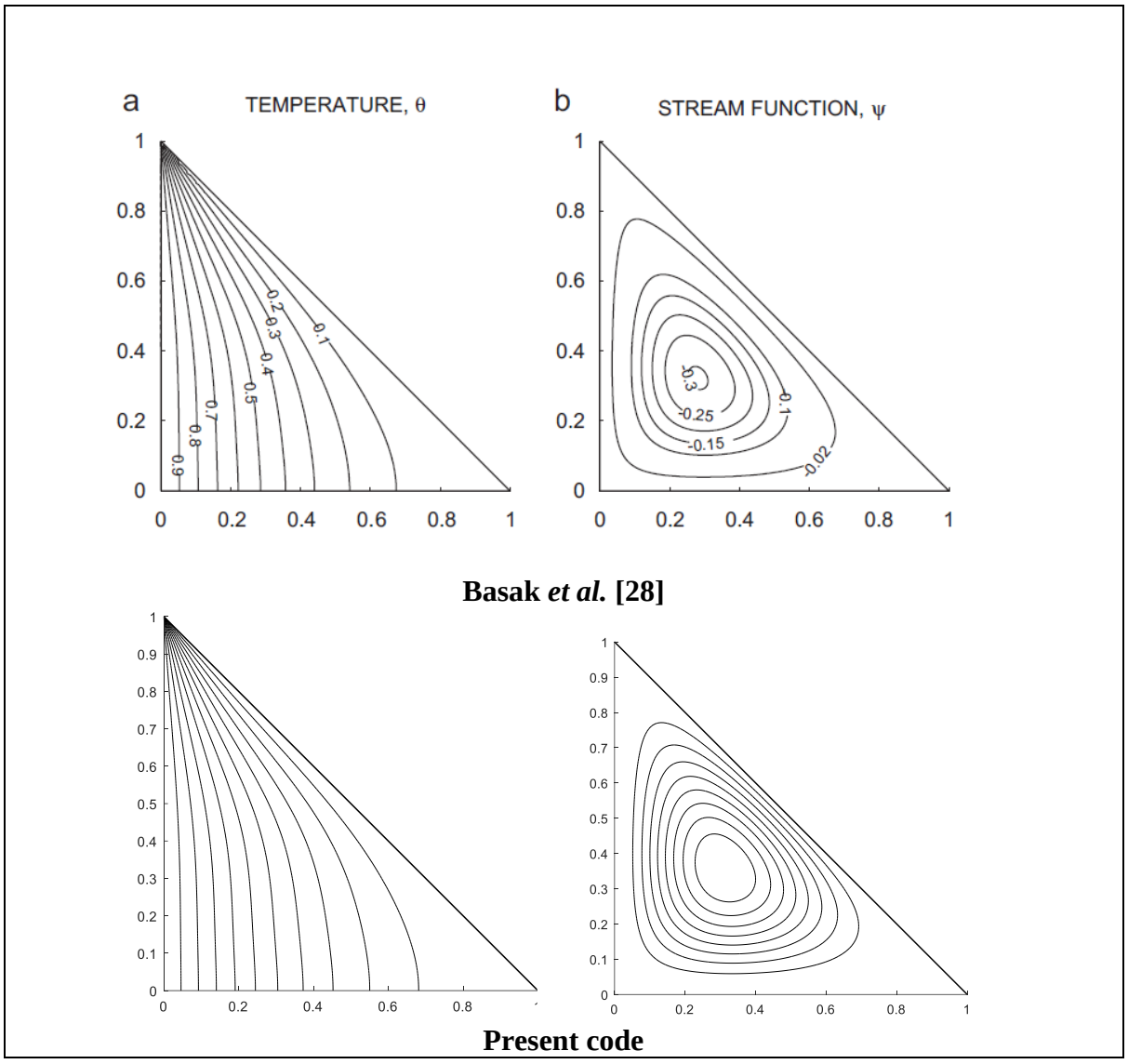

Fig.2. Comparison of temperature and streamline contour plots with Basak *et al.* [28] for uniformly heated left vertical wall, $\theta(0,\mathrm{Y})=1$ and cooled right inclined wall, $\theta(\mathrm{X},\mathrm{Y})=0$, $\forall$ $X+Y=1$ and insulated bottom wall with $Ra=10^3$ *and* $Pr=0.71$, $Ha=0$ *and* $Da\to\infty$.

Dimensionless stream function ψ and vorticity ω are defined as:

$$U=\frac{\partial\psi}{\partial Y},\ V=-\frac{\partial\psi}{\partial X} \tag{11}$$

$$\omega=\frac{\partial V}{\partial X}-\frac{\partial U}{\partial Y}=-\frac{\partial^2\psi}{\partial X^2}-\frac{\partial^2\psi}{\partial Y^2} \tag{12}$$

The required vorticity transport equation is obtained from the differentiation of the *x*-momentum equation with respect to *y, and* the *y*-momentum equation with respect to *x* and then subtracting the resulting equations leads to:

$$\frac{\partial \omega}{\partial \tau}+U\frac{\partial \omega}{\partial X}+V\frac{\partial \omega}{\partial Y}=\Pr\left(\frac{\partial^2 \omega}{\partial X^2}+\frac{\partial^2 \omega}{\partial Y^2}\right)-\frac{\Pr}{Da}\omega-HA^2\Pr\frac{\partial V}{\partial X}+Ra.\Pr\frac{\partial \theta}{\partial X} \quad (13)$$

$$\frac{\partial \theta}{\partial \tau}+U\frac{\partial \theta}{\partial X}+V\frac{\partial \theta}{\partial Y}=\left(\frac{\partial^2 \theta}{\partial X^2}+\frac{\partial^2 \theta}{\partial Y^2}\right) \quad (14)$$

The corresponding boundary conditions are:

On the Left (vertical) wall: $X=0, U=V=\psi=0, \frac{\partial \theta}{\partial X}=0, \omega=-\frac{\partial^2 \psi}{\partial X^2}$

On the bottom wall: $Y=0, U=V=\psi=0, \theta=1, \omega=-\frac{\partial^2 \psi}{\partial Y^2}$

On the inclined wall: $U=V=\psi=0, \theta=0, \omega=-\frac{\partial^2 \psi}{\partial n^2}$ (15)

In the above equations, the key dimensionless parameters arising are defined as:

$$Ha=B_0 L\sqrt{\frac{\sigma}{\mu}},\ Ra=\frac{g\beta\left(T_h-T_c\right)L^3}{\alpha\nu},\ Da=\frac{K}{L^2},\ \Pr=\frac{\nu}{\alpha}$$

All terms are defined in the nomenclature.

3. NUMERICAL SOLUTION PROCEDURE

The non-linear coupled governing equations (13) and (14) and the corresponding boundary conditions (15) describing the hydromagnetic Darcian natural convection flow in the enclosure (domain) are employed numerically with a robust finite difference method. The details of the finite difference procedure are described at length in earlier studies by the authors [29-35]. The stream function is evaluated from Eqn. (12) and it is discretized with a five-point difference scheme using central difference approximations. The convective terms in the momentum conservation equations are discretized with *second order* accuracy. A central finite difference scheme is also implemented to approximate the diffusive terms with uniform spacing along the *X and Y*-directions (as depicted in the grid design shown in **Fig. 1b**). The present in-house computational fluid dynamics (CFD) MATLAB code has been refined successfully with the earlier *non-magnetic*, *non-porous* (*Ha* = 0, *Da* $\rightarrow\infty$) finite element study of Basak *et al.* [28]. The comparisons for fluid flow patterns and isotherms contours are presented in **Fig. 2** and excellent correlation is achieved.

Table 1

Comparison between the present Nusselt number with the ones of Varol et. Al [36] for a triangular enclosure.

Ra	**10^3**	**10^4**	**10^5**	**10^6**
Varol et. al [36]	5.508	2.891	1.395	1.039
Present work	5.532	2.912	1.397	1.045
Error (%)	0.4357	0.7264	0.1434	0.5774

Table 2

The impact of different grid resolutions on the Average Nusselt number Nu of the hot wall is evaluated for Ra = 10^5, Pr=0.71, Da = 0.1 and Ha = 20.

Grid size	**40X40**	**60X60**	**80X80**	**120X120**
Avg_Nu	4.6715	4.6722	4.6723	4.6722

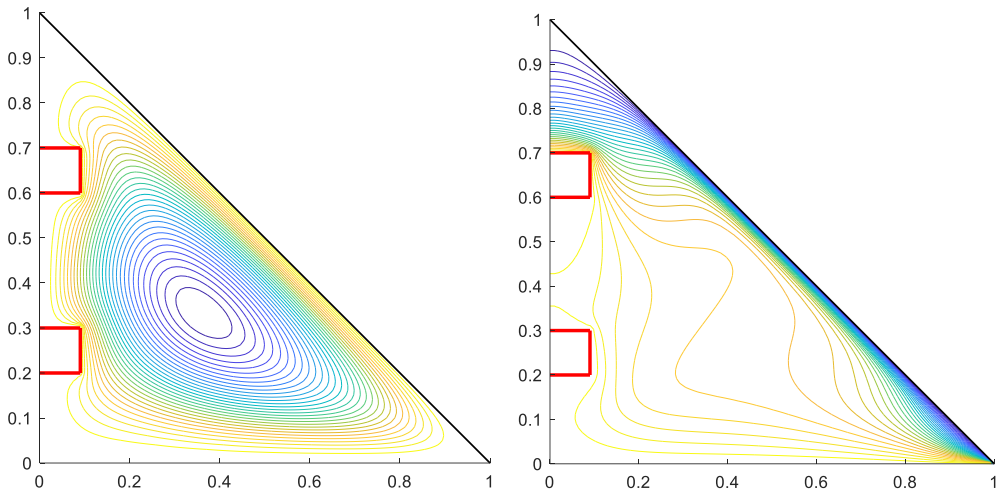

Fig.3. Contour plots for streamlines and isotherms with ***Da = 0.1***, *Ra =10^5, Pr = 0.71, Ha = 5.*

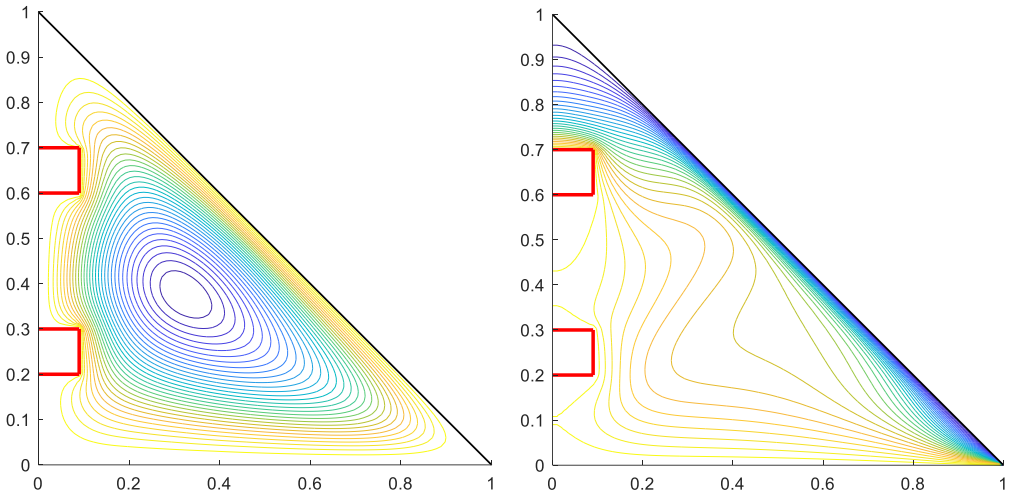

Fig.4. Contour plots for streamlines and isotherms with ***Da = 0.01***, $Ra = 10^5$, $Pr = 0.71$, $Ha = 5$.

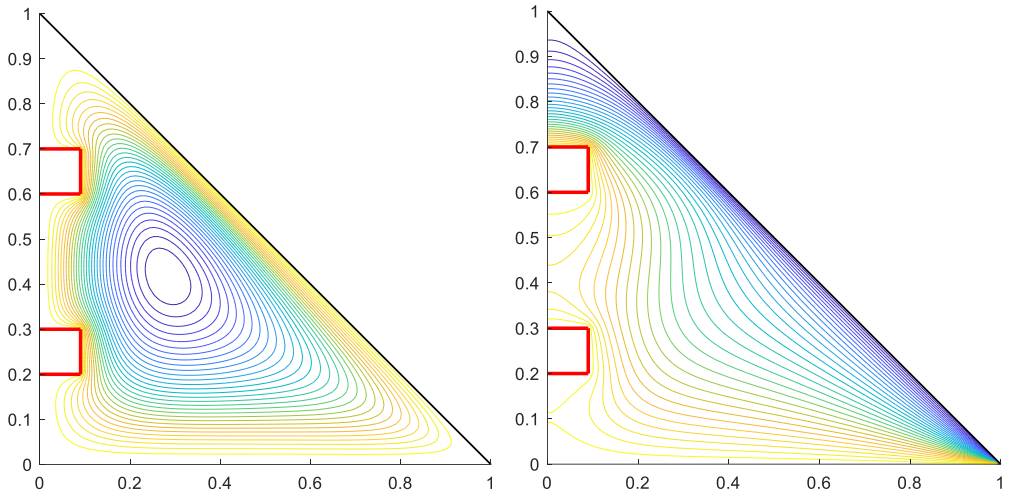

Fig.5. Contour plots for streamlines and isotherms with ***Da = 0.001***, $Ra = 10^5$, $Pr = 0.71$, $Ha = 5$.

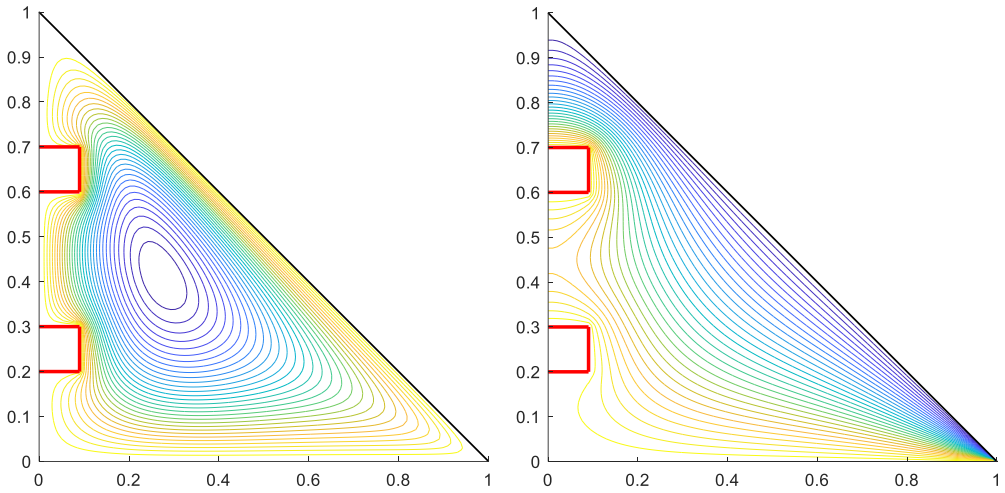

Fig.6. Contour plots for streamlines and isotherms with ***Da* = *0.0001***, *Ra* =10^5, *Pr* = *0.71*, *Ha* = *5*.

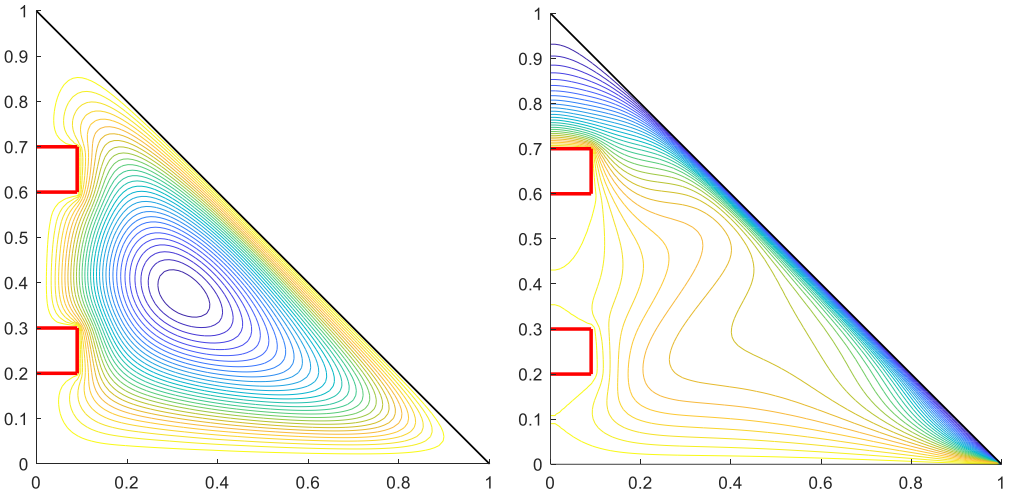

Fig.7. Contour plots for streamlines and isotherms with *Da* = *0.1*, *Ra* =10^5, *Pr* = *0.71*, ***Ha* = *5*.**

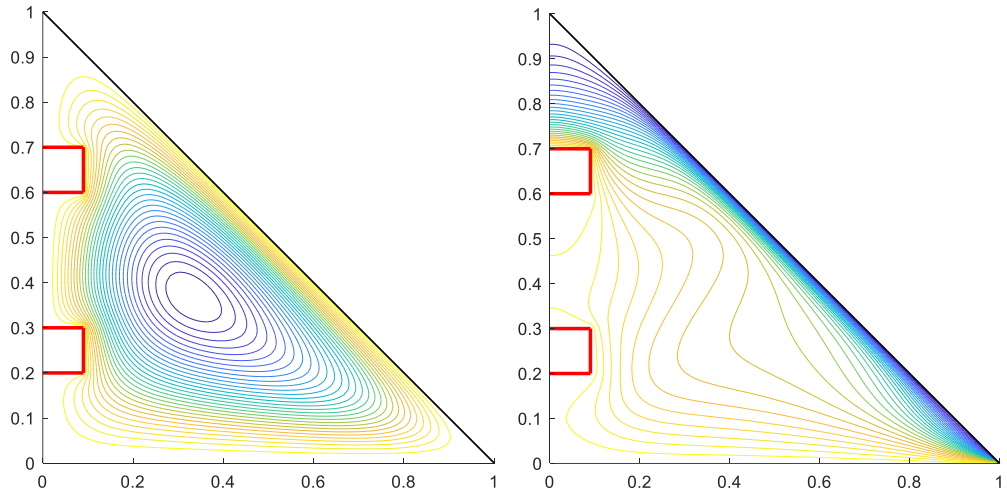

Fig.8. Contour plots for streamlines and isotherms with $Da = 0.01$, $Ra = 10^5$, $Pr = 0.71$, $\boldsymbol{Ha = 10}$.

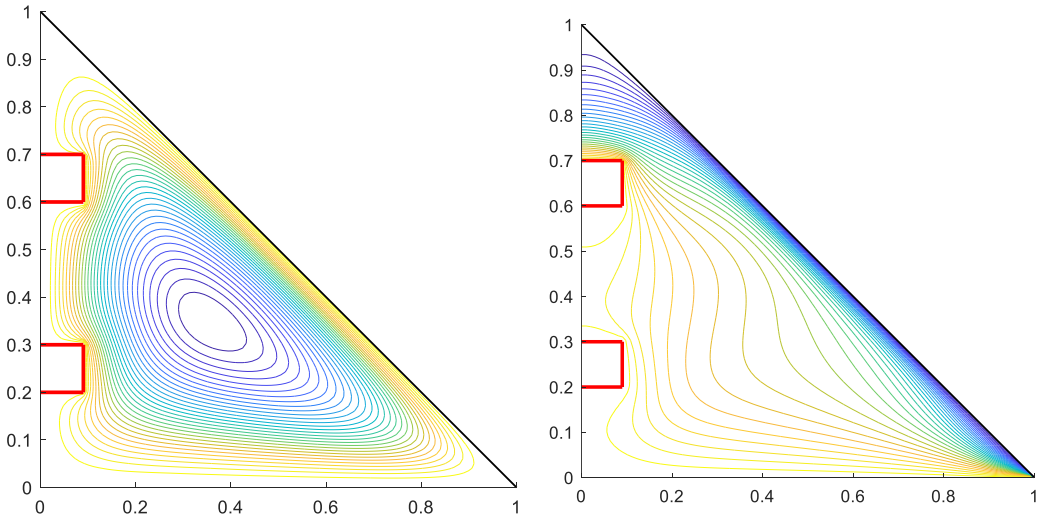

Fig.9. Contour plots for streamlines and isotherms with $Da = 0.01$, $Ra = 10^5$, $Pr = 0.71$, $\boldsymbol{Ha = 20}$.

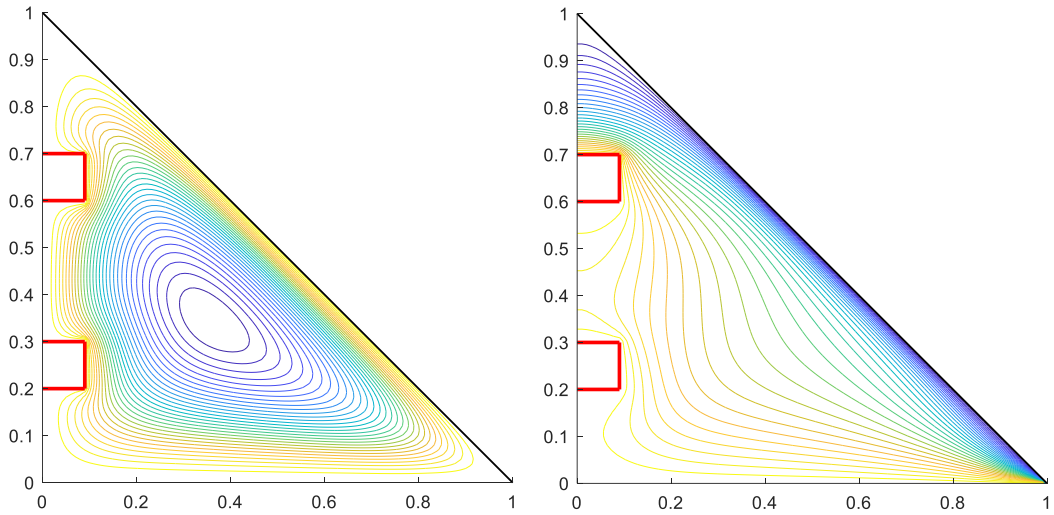

Fig.10. Contour plots for streamlines and isotherms with $Da = 0.01$, $Ra = 10^5$, $Pr = 0.71$, $\boldsymbol{Ha = 30.}$

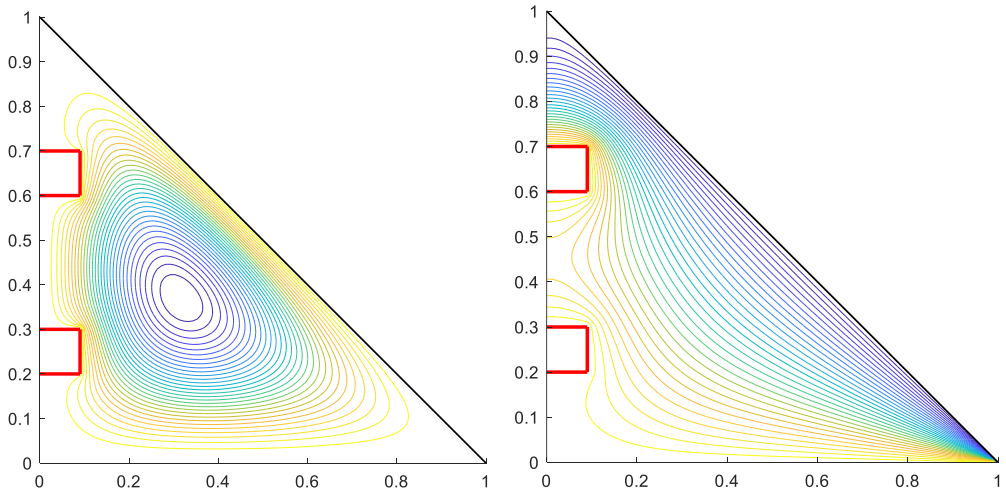

Fig.11. Contour plots for streamlines and isotherms with $Da = 0.1$, $\boldsymbol{Ra = 10^3}$, $Pr = 0.71$, $Ha = 5.$

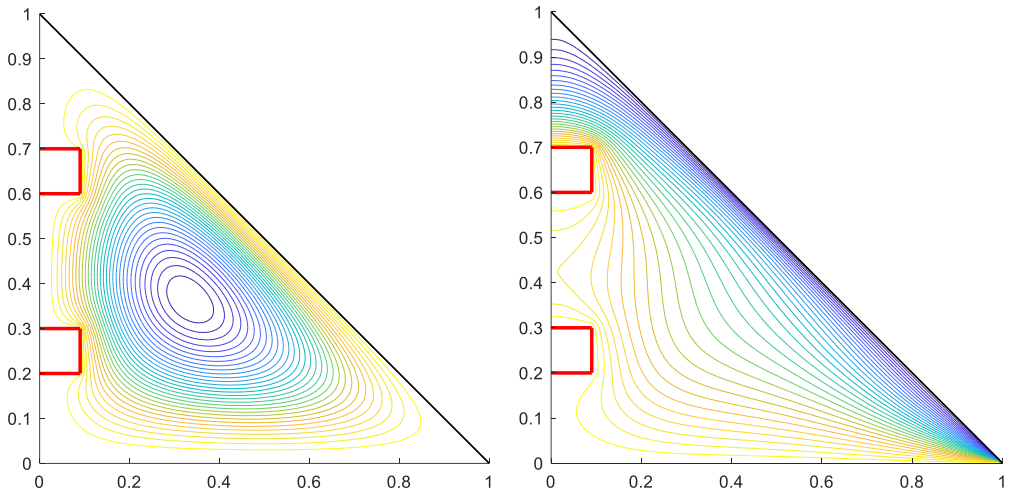

Fig.12. Contour plots for streamlines and isotherms with $Da = 0.1$, $\boldsymbol{Ra = 10^4}$, $Pr = 0.71$, $Ha = 5$.

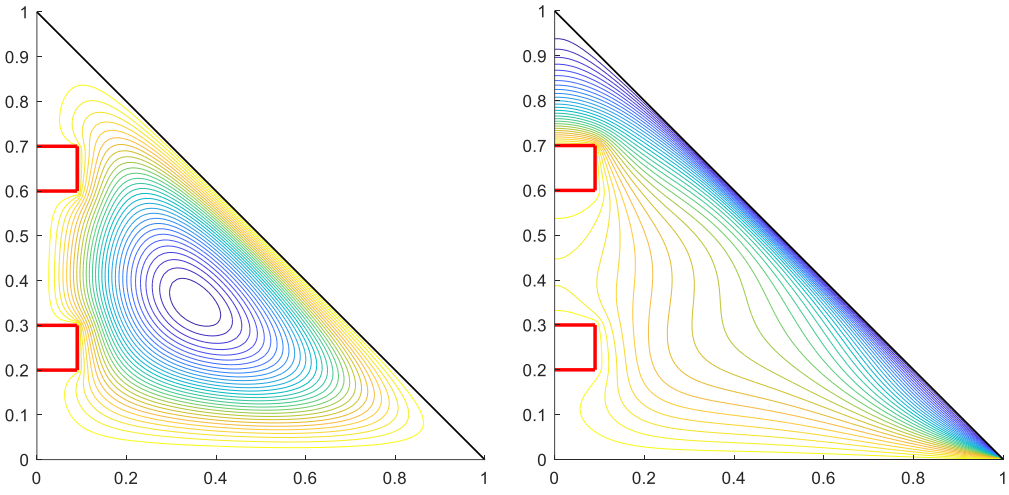

Fig.13. Contour plots for streamlines and isotherms with $Da = 0.1$, $\boldsymbol{Ra = 2\ X\ 10^4}$, $Pr = 0.71$, $Ha = 5$.

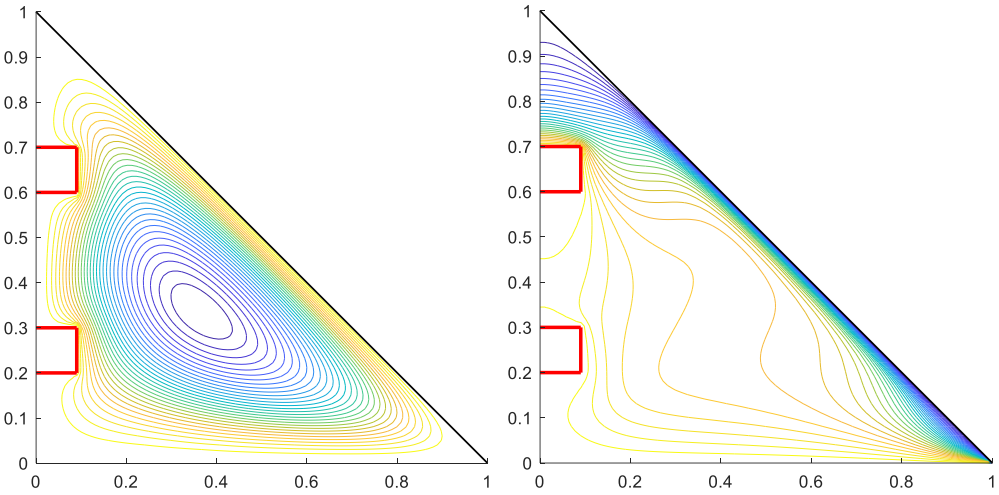

Fig.14. Contour plots for streamlines and isotherms with *Da = 0.1,* ***Ra =10^5,*** *Pr = 0.71, Ha = 5.*

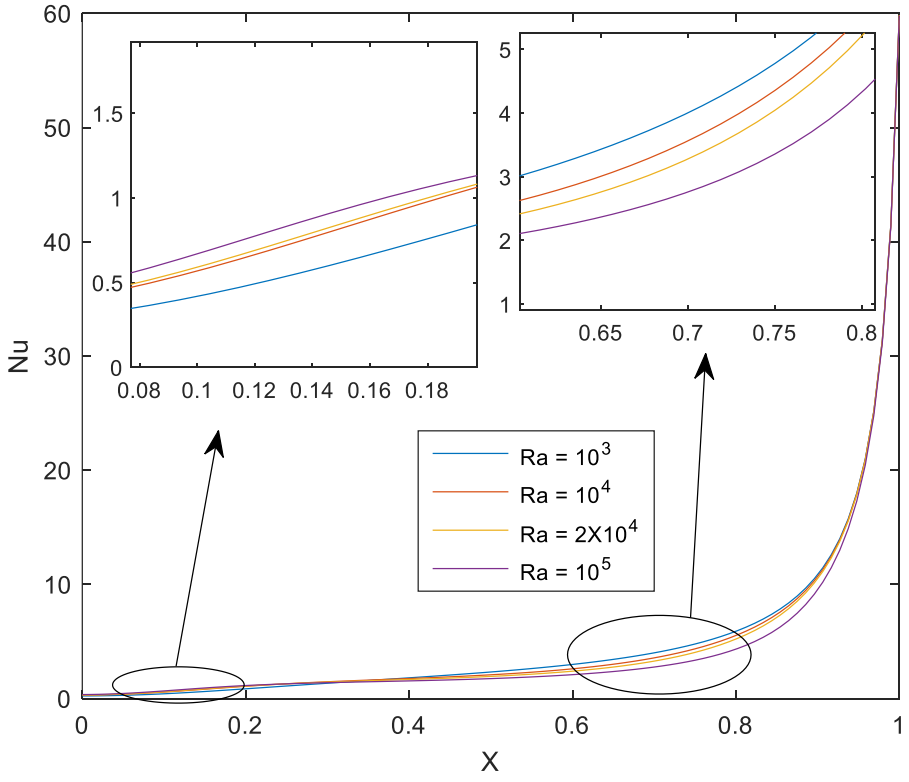

Fig.15. Local Nusselt number along the hot wall for *Da = 0.1, Pr = 0.71, Ha = 5.*

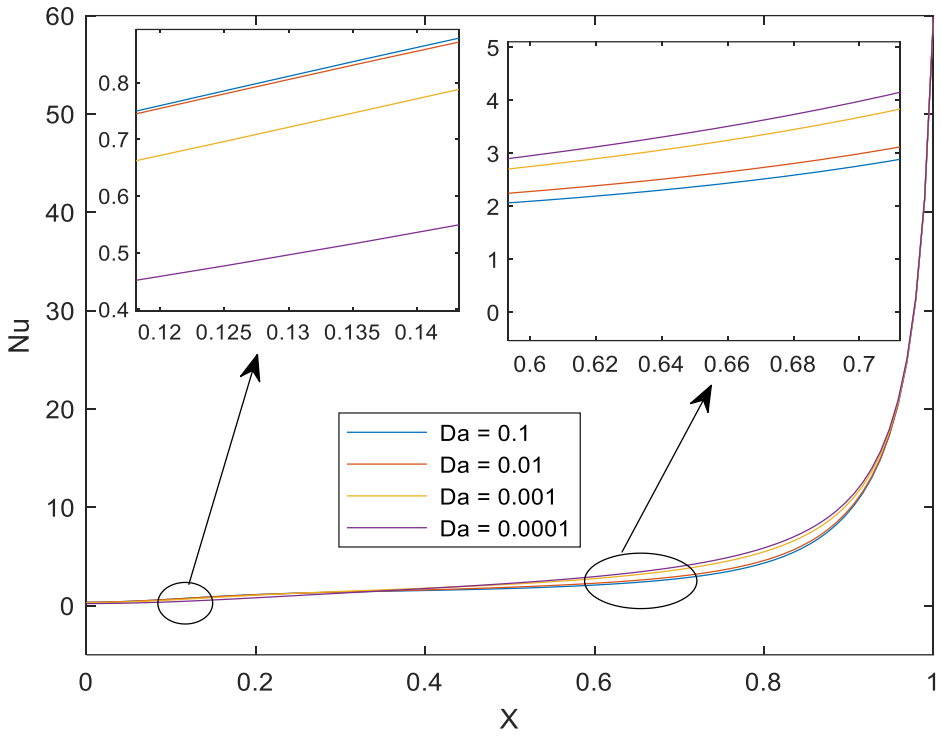

Fig.16. Local Nusselt number along the hot wall for ***Ra* =10⁵,** *Pr = 0.71, Ha = 5.*

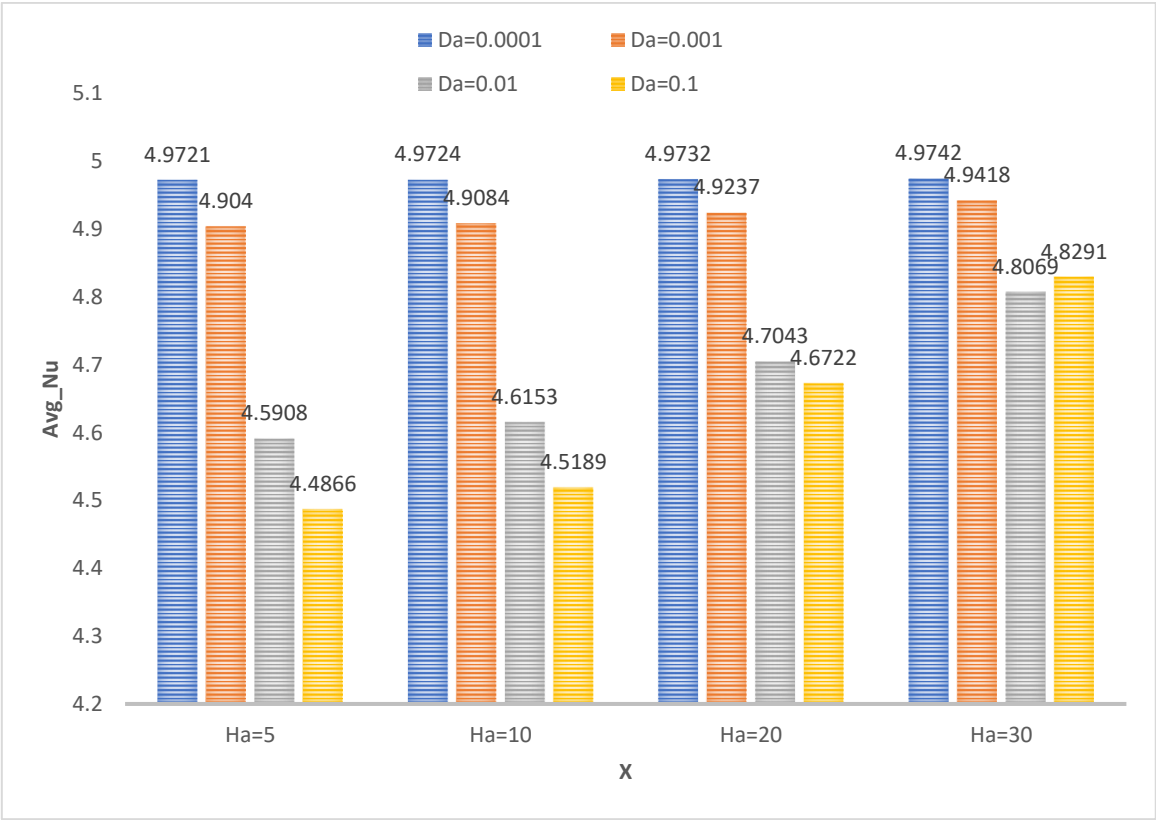

Fig.17. Average Nusselt number along the hot wall for ***Ra* =10⁵,** *Pr = 0.71.*

In order to verify the code and ensure its accuracy, the numerical findings are compared with the ones obtained by Varol et. al [36]. They studied a triangular enclosure saturated with the air as a hot source at constant temperature was located at the bottom of vertical wall of the cavity. The results are compared in **Table 1.** The differences between the findings are acceptable due the approximations that the researchers consider in the discretization and averaging.

Now, the grid independency is investigated to choose an appropriate grid resolution. To reach this goal, the influence of the number of grid points on the Nu of the hot wall is evaluated for Ra = 10^5, Pr=0.71, Da = 0.1 and Ha = 20. The results are presented in Table 2. As Table 2 shows that further rise of the grid resolution of 120 × 120 does not impact the average Nu. So, in order to save time and computational costs, this grid resolution is selected for more simulations.

4. DISCUSSION

The numerical simulations have been conducted and are depicted in **Figs. 3-17**. In all cases Prandtl number (*Pr*) is constrained as 0.71 (electrically conducting air). The two identical obstacles are prescribed temperatures of $\theta = 1$ i.e. they act as heat sources located along the adiabatic vertical wall.

Figs. 3a, b- 6a, b demonstrates the streamlines and isotherm topologies for progressively diminishing values of Darcy number, Da. In all cases the presence of the two heat source obstacles at the vertical wall deflects the single vortex cell structure further from the vertical wall. At higher Darcy numbers (*Da* = 0.1 and 0.01 in Figs. 3a, 4a, respectively) the vortex is diagonally stretched from the top left corner to the lower right corner. However, as *Da* is elevated further, the vortex structure migrates further towards the upper left corner and expands laterally. There is an intensification in circulation towards the left vertical wall and a relaxation in the lower right corner, above the hot base wall. Higher *Da* values imply increased permeability of the porous medium which permits easier percolation of the magnetized air in the enclosure. The Darcian impedance terms are decreased with greater *Da* values. This results in a more homogenous distribution of streamlines and the vortex cell. However, at lower Da, the permeability is significantly reduced in the regime and greater resistance is offered via the solid fibers. This introduces asymmetry into the circulation in the enclosure and a stretching in the diagonal direction from the top left corner with constriction arising. The isotherms are also

modified significantly with decrement in medium permeability. The colder zones associated with the inclined boundary progressively encroach deeper into the interior of the enclosure and dominate the upper left corner zone. The warmer zones are pushed towards the vertical wall, although the presence of the obstacles increasingly distorts the isotherm structure and at very low permeability significant intensification in isotherm distribution is computed in the vicinity of the vertical adiabatic wall. In high permeability (high Da) cases there is substantial warping of the isotherms in the central zone but this is progressively stifled and isolated towards the obstacles only at higher permeability. Thermal conduction in the regime is progressively elevated with lower permeability (greater concentration of solid fibers in the cavity) and the presence of obstacles sustains a good temperature distribution at least near the vertical wall. Higher temperatures are consistently observed near the upper section of the upper obstacle and also good temperatures are sustained near the lower base hot wall.

Figs. 7a, b- 10a, b shows the impact of Hartmann (magnetic) number, *Ha*, on streamline (isovelocity) and temperature distributions. With increment in Hartmann number from 5 through 10, 20, 30, the single vortex cell in the enclosure is progressively stretched in the inclined direction from the upper left corner to the lower right corner. The streamlines relax and this indicates a deceleration in the flow which is associated with the damping effect of a transverse magnetic field. Although the Lorentzian force acts only in the vertical direction (the magnetic field is orientated parallel to the base wall), the effect is significant on the entire flow field. The implication is that momentum is successfully re-distributed in the regime with magnetic field and this assists in producing a more homogenous velocity field of relevance to materials processing operations. The isotherms undergo significant warping at lower *Ha* values in particular in the central zone. The cold inclined wall zone is however reduced with greater magnetic field effect since the supplementary work expended by the fluid in dragging against the action of the magnetic field is dissipated as thermal energy. This generates heat in the regime and expands the isotherms producing a more balanced temperature distribution in which the central zone isotherms are more vertically aligned at higher Ha then they are at lower Ha values. Again, temperatures are higher at the upper obstacle top surface with highest temperatures computed in this vicinity, although a cold zone is still sustained in the uppermost section of the top left corner of the enclosure.

Figs. 11a, b- 14 a, b displays the impact of Rayleigh number, *Ra*, on streamline (isovelocity) and isotherm plots. As *Ra* is increased from 10^3 through 10^4 to 2 x 10^4 and finally 10^5, there is a substantial elongation computed in the single vortex cell in the enclosure. The vortex is

stretched again in the diagonal direction from the upper left corner to the lower right corner and expands significantly. This implies a reduction in momentum and decrease in velocity in the regime, which is characteristic with higher thermal buoyancy effects (Rayleigh number expresses the ratio of buoyancy and viscous drag force in the regime). Velocities in the central zone are reduced whereas they are elevated in the peripheral zones with increased Rayleigh number. At lower Rayleigh number (fig. 11a, $Ra = 10^3$) the temperature lines are generally parallel to the inclined wall and only distorted markedly near the obstacles as we approach the left vertical adiabatic wall. However, with increasing *Ra*, this distortion is amplified in the central zone and simultaneously hotter zones push further towards the inclined cold wall. The cold (blue) zone at the inclined wall is constricted significantly with stronger thermal buoyancy effect (higher Rayleigh number) and although the isotherms are increasingly warped in the central zone, the temperatures are much higher (yellow and green zones). As before highest temperatures are computed near the upper obstacle but are not confined to the top surface, and now encompass all three sides of this obstacle. Higher temperatures are also observed in the vicinity of the lower obstacle although the intensification is weaker than at the upper obstacle.

Figs. 15- 17 depict the effect of dissimilar parameters on the local Nusselt number at the hot base wall and also the average Nusselt number. These parameters are defined respectively as:

Local Nusselt number i.e. non-dimensional heat transfer rate at the hot base *wall*:

$$Nu = \frac{qH}{k(T_h - T_c)} = -[\frac{\partial \theta}{\partial X}]_{X=1} \tag{17}$$

Average Nusselt number, designated by avg_*Nu* at the hot base wall:

$$Avg\_Nu = \int_0^1 Nu dy \tag{18}$$

With elevation in Rayleigh number (**Fig. 15**) there is an increment in local Nusselt number initially at low values of *X* i.e. closer to the left vertical adiabatic wall in the range $0 < X < 0.2$. However soon this trend is reversed, and a strong decrement is computed in Nusselt number for the remaining length of the base wall. The amplification in thermal buoyancy effect associated with greater Rayleigh numbers produces heating of the enclosure fluid. This reduces the transfer of heat from the core fluid to the boundaries (walls) and explains the associated decrease in local Nusselt number with *X*-values as we progress along the base wall. However irrespective of the Rayleigh number, Nusselt number ascends with greater values of *x* owing to the nature of the hot base wall. **Fig. 16** shows that initially the local Nusselt number is boosted

with increment in Darcy number at low values of X along the base hot wall; however for the majority of the extent of the wall ($0.4<X<1$) the contrary behaviour is computed and local Nusselt number is suppressed with increasing Darcy number i.e. heat transfer rate to the base wall is decreased with greater permeability of the porous medium. In both Figs. 15 and 16, relatively strong magnetic field is considered i.e. $Ha = 5$.

Fig. 17 indicates that average Nusselt number is generally increased at the lower hot base wall with lower Darcy number (peak values in the histogram correspond to $Da = 0.0001$ at any value of Hartmann number, Ha). The converse response is computed for high Darcy number. Significantly higher values of average Nusselt number are produced with an increment in Hartmann number but only at higher Darcy number ($Da = 0.01$ and 0.1). At lower Darcy number there is no tangible modification in the average Nusselt number with increasing Hartmann numbers. Magnetic field therefore is found to encourage heat transfer to the lower base hot wall only for greater permeability of the porous medium.

---

5. CONCLUSIONS

A two-dimensional mathematical model has been presented for the laminar viscous magnetohydrodynamic natural convection flow in a triangular regime containing a porous medium saturated with electrically conducting air and containing hot obstacles. A magnetic strength is imposed parallel to the base wall. The pressure gradient term is eliminated by using the vorticity-stream function approach. The emerging dimensionless governing equations along the boundary conditions have been employed by the finite difference scheme with validation included for the special case of non-magnetic, no-porous flow as available in the literature. The impact of fluid and thermal parameters on streamlines, temperature contours, local and average Nusselt numbers (at the base wall) for emerging parameters have been visualized graphically. The principal findings of the present numerical examination may be listed as follows.

(i) Increasing Hartmann number (magnetic field) elevates the average Nusselt number at the lower base hot wall but only with higher Darcy numbers (greater permeability of the porous medium).

(ii) A significant decrease is computed in local Nusselt number for the majority of the extent of the base wall with greater thermal buoyancy effect (higher Rayleigh numbers).

(iii) With increasing Rayleigh number, there is a substantial elongation computed in the single vortex cell in the enclosure and velocities in the central zone are reduced whereas they are enhanced in the peripheral zones with increased Rayleigh number.

(iv) At lower Rayleigh number the isotherms are generally parallel to the inclined wall and only distorted substantially near the obstacles at the left vertical adiabatic wall; however, with increasing *Rayleigh number*, this distortion is magnified in the core zone and simultaneously warmer zones expand towards the inclined cold wall.

(v) With greater Hartmann number (stronger magnetic field) the single vortex cell in the enclosure is progressively elongated in the diagonal direction from the upper left corner to the lower right corner and strong damping is generated.

(vi) With increasing Darcy number, the vortex cell migrates towards the upper left corner and expands laterally, with an associated intensification in circulation towards the left vertical wall and a relaxation in the lower right corner, above the hot base wall.

The present simulations have revealed some interesting characteristics of heat and momentum transfer in triangular enclosure hydromagnetic porous media convection under buoyancy forces. However magnetic induction effects have been neglected. These may be considered in the future and the finite difference technique adopted appears to hold excellent promise in simulating such flows.

REFERENCES

[1] Wi Liu, Amin Shahsavar, Azeez A. Barzinjy, Abdullah A.A.A. Al-Rashed, Masoud Afrand, *International Communications in Heat and Mass Transfer,* 108, 104309 (2019),.

[2] Debayan Das, Leo Lukose, Tanmay Basak, *International Journal of Heat and Mass Transfer* 127, 1290–1312 (2018).

[3] Omid Mahian, Ali Kianifar, Saeed Zeinali Heris, Somchai Wongwises, *International Journal of Heat and Mass Transfer* 99, 792–804 (2016).

[4] Feroz Ahmed Soomro, Rizwan Ul Haq, Ebrahem A. Algehyne, Iskander Tlili, , *Journal of Energy Storage* 31, 101702 (2020).

[5] Mohsen Izadi, *Chinese Journal of Chemical Engineering* 28, 1203–1213, (2020),

[6] Selimefendigil, F., & Öztop, H. F. *Journal of the Taiwan Institute of Chemical Engineers*, *45*(5), 2150-2162 (2014).

[7] Kent, E. F., Asmaz, E., & Ozerbay, S., *Heat and Mass Transfer*, *44*(2), 187-200 (2007).

[8] Ahmed, S. E., Mansour, M. A., Rashad, A. M., & Salah, T., *Journal of Thermal Analysis and Calorimetry*, *139*(5), 3133-3149 (2020).

[9] Varol, Y., *International Communications in Heat and Mass Transfer*, *38*(3), 368-376 (2011).

[10] Bég, O. A, Kuharat, S, Kadir, A and Jouri, W. *Materials of the Future: Smart Applications in Science and Engineering*, Qatar University, Doha, Qatar, March 29-31. (2021),

[11] M. H. Khan, K. Venkatadri, O. Anwar Bég, V. R. Prasad, B. Mallikarjuna, *Int. J Applied Comp. Mathematics*, 4, 61, 1-20 (2018).

[12] Bég, O. A., Venkatadri, K., Prasad, V. R., Beg, T. A., Kadir, A., & Leonard, H. J. *Materials Science and Engineering: B*, *261*, 114722 (2020).

[13] O. Anwar Bég, K. Venkatadri, V.R. Prasad, Tasveer A. Bég, Henry J. Leonard, W.S. Jouri, *Proc. IMechE-Part C – J. Mechanical Engineering Science (2020).*

[14] S. Kuharat, O. Anwar Bég, Ali Kadir and B. Vasu, *Arabian J. Science and Engineering (2020). (19 pages).*

[15] Das, D., & Basak, T., *International Journal of Heat and Mass Transfer*, 112, 489–508 (2017).

[16] Fayz-Al-Asad, Md., Nur Alam, Md., Ahmad, H., Sarker, M.M.A., Alsulami, M.D., Gepreel, K.A., *Results in Physics* (2021).

[17] Z. Li, A. Shahsavar, K. Niazi, A.A.A.A. Al-Rashed, P. Talebizadehsardari, *Powder Technology* (2019).

[18] Yesiloz, G., & Aydin, O., *International Journal of Heat and Mass Transfer*, *60*, 365-374 (2013).

[19] Ahmed, S. E., Rashad, A. M., & Reddy Gorla, R. S. Journal of Thermophysics and Heat Transfer, 27(4) (2013).

[20] Chowdhury, R., Parvin, S., & Khan, M. A. H. *Heliyon*, *2*(8), e00140 (2016).

[21] M.M. Rahman *et al., International Communications in Heat and Mass Transfer* 39, 78-84 (2012).

[22] C. Sivaraj and M.A.Sheremet, *Journal of Magnetism and Magnetic Materials*, 426, 351-360 (2017).

[23] Hiroyuki Ozoe (Ed)., *Magnetic Convection*, 236 pp, Imperial College Press (2005).

[24] C. Jiang et al., *J Supercond Nov Magn* 27, 519–525 (2014)

[25] C. Jiang *et al., Journal of Magnetism and Magnetic Materials*, *357*, 53-60 (2014).

[26] S. Bouabdallah and R. Bessaïh, *Fluid Dynamics & Materials Processing*, Vol.6, No.3, pp. 251-276 (2010).

[27] Imen Mejri *et al., Fluid Dynamics & Materials Processing*, Vol.10, No.1, pp. 83-114 (2014).

[28] Basak, T., Roy, S., & Thirumalesha, C. *Chemical Engineering Science*, 62(9), 2623–2640 (2007).

[29] K. Venkatadri, O. Anwar Bég, P Rajarajeswari, V. Ramachandra Prasad, *International Journal of Mechanical Sciences* 171 105391 (2020).

[30] Venkatadri K, Gouse Mohiddin S, Suryanarayana Reddy M., *Engineering Computations*, 34 (8), 2463-2478 (2017).

[31] Venkatadri, K., Shobha, A., Venkata Lakshmi, C., Ramachandra Prasad, V., Hidayathulla Khan, B. *Journal of Computational Applied Mechanics*, 51 (2), 323-331 (2020).

[32] T Sarala Devi, C Venkata Lakshmi, K Venkatadri, V Ramachandra Prasad, O. Anwar Bég, M. Suryanarayana Reddy. *Heat Transfer* 49 (4), 1769-1787 (2020).

[33] Venkatadri, K., Gaffar, S., Prasad V., R., Hidayathulla Khan, B. M., & Anwar Bég, O. *International Journal of Automotive and Mechanical Engineering*, *16*(4), 7375-7390 (2019).

[34] K. Venkatadri, S. Abdul Gaffar, M. Suryanarayana Reddy, V. Ramachandra Prasad, B.Md. Hidayathulla Khan, O. Anwar Bég,. *Journal of Applied and Computational Mechanics* 6(1), 52-62 (2020).

[35] K. Venkatadri, O. Anwar Bég, P Rajarajeswari, V. Ramachandra Prasad, A. Subbarao, B. Md. Hidayathulla Khan, , *Journal of Porous Media*, 23(12), 1187-1199 (2020).

[36] Afrand, M., Pordanjani, A. H., Aghakhani, S., Oztop, H. F., & Abu-Hamdeh, N. *International Communications in Heat and Mass Transfer*, *112*, 104507 (2020).

[37] Al-Farhany, K., Alomari, M.A., Saleem, K.B. *et al.*. *Eur. Phys. J. Plus* **136,** 814 (2021).

[38] Doostali, A., Rezazadeh, M. *Eur. Phys. J. Plus* **133,** 511 (2018).